Numerical Solution of a Nonlinear Evolution Equation Describing Amorphous Surface Growth of Thin Films

Ronald H.W. Hoppe[1,2] and Eva Nash[3]

[1] Department of Mathematics, University of Houston, Houston TX 772004-3008, U.S.A.
[2] Institute for Mathematics, University of Augsburg, D-86159 Augsburg, Germany
[3] Infineon Technologies AG, D-81541 Munich, Germany

Summary. We consider a nonlinear parabolic partial differential equation that describes the evolution of the surface morphology in the deposition of thin glassy films by molecular beam epitaxy. The dynamics of the growth process exhibits some unexpected initial linear behavior, before the nonlinear dynamics sets in. Therefore, for the numerical solution we suggest a combined spectral element/finite element approach. Results of numerical simulations are given that show a good agreement with experimental measurements.

1 Introduction

We consider the deposition of thin glassy films on the surface of substrates such as silicon by molecular beam epitaxy. Such processes play an important role in materials science with regard to the coating of surfaces in order to obtain specific surface properties (cf., e.g., [11]).
In particular, we assume that the particle beam is impinging perpendicularly to the surface of the substrate (cf. Fig. 1).
Denoting by $\Omega := [0, L]^2 \subset \mathbb{R}^2$ the surface of the substrate, the deposition process can be described by the temporal and spatial distribution of the height profile $u(x,t)$, $x \in \Omega$, $t \geq 0$, as given by

$$u(x,t) \;=\; H(x,t) \;-\; F\, t\;, \tag{1}$$

where $H(x,t)$ is the absolute height and F refers to the deposition rate which is assumed to be constant.
As far as the development of an appropriate mathematical model is concerned, the deposition evolves according to

$$\frac{\partial u}{\partial t}(x,t) \;=\; g(u(x,t)) \quad , \quad x \in \Omega\;,\; t \geq 0 \tag{2}$$

where the right-hand side g describes the surface growth. There have been many attempts to establish appropriate models for the morphology of deposition processes featuring amorphous surface growth (cf., e.g., [1, 4, 13]). Here,

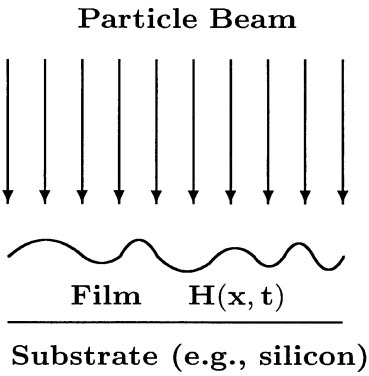

Fig. 1. Schematic representation of the deposition of thin films

following [5, 10] and [11], we take three major growth mechanisms into account:
The first one describes surface growth due to particle interaction

$$g_1(u) \;:=\; -\,S\,(1 \,+\, |\nabla u|^{3/2})^{-1}\,\Delta u\;, \tag{3}$$

where S stands for the influence of interatomic and van der Waals forces.
The second one is curvature induced surface relaxation

$$g_2(u) \;:=\; -\,D\,\nabla\,\big[\,(1 \,+\, |\nabla u|^2)^{-1/2}\,\nabla\,((1 \,+\, |\nabla u|^{3/2})^{-1}\,\Delta u)\,\big]\;. \tag{4}$$

Here, D refers to the material dependent diffusion coefficient.
Finally, the third mechanism is due to structure coarsening in the sense that particles at locations with high gradients of the height profile move to locations with lower gradients. Here, we follow the model suggested by Moske (see [11])

$$g_3(u) \;:=\; C\,\big[\,(1 \,+\, |\nabla u|^2)^{-1/2}\,\nabla\,(1 \,+\, |\nabla u|^2)^{-1/2}\,\big]\;, \tag{5}$$

where C denotes the mean surface mobility.
As long as the particle beam impinges perpendicularly onto the surface of the substrate, we have $|\nabla u| \ll 1$. In this case, the functions $g_i = g_i(u), 1 \le i \le 3$, in (3),(4), and (5) simplify to

$$g_1(u) \;:=\; a_1\,\Delta^2 u\;,\; g_2(u) \;:=\; a_2\,\Delta u\;,\; g_3(u) \;:=\; a_3\,\Delta(|\nabla u|^2)\quad,$$

where $a_i < 0\;,\; 1 \le i \le 3$. The evolution equation takes the form

$$\frac{\partial u}{\partial t} \;=\; \Delta(a_1 u \,+\, a_2\Delta u \,+\, a_3|\nabla u|^2)\quad \text{in } Q := \Omega \times [0,\infty) \tag{6}$$

with an initial condition $u(x,0) = u_0(x)\;,\; x \in \Omega$, and either periodic boundary conditions or homogeneous Neumann boundary conditions on $\Gamma = \partial\Omega$.

The constants a_1, a_2 and a_3 in the evolution equation are usually determined by parameter identification with respect to experimentally obtained measurements by using Auger spectroscopy and scanning electron microscopy .
However, if the particle beam does not impinge perpendicularly, there are overhangs in the profile and even topological changes due the formation of inclusions. In this case, we must use the original form of the functions $g_i = g_i(u)$, $1 \leq i \leq 3$, as given by (3), (4), (5), and resort to other techniques as, for instance, level set methods (cf., e.g., [8, 9]; see also [3]).
We note that the nonlinear 4th order evolution equation (6) resembles the well-known Cahn-Hilliard equation which describes spinodal decomposition, i.e., phase separation in binary alloys (cf., e.g., [6]).
The paper is organized as follows: In section 2, we will briefly address the dynamics of the growth process which features some unexpected initial linear behavior. This motivates the use of a combined spectral element/finite element approach for the numerical solution of the nonlinear evolution equation (6) that is described in sections 3 and 4. Finally, in section 5 we will give some simulation results in terms of visualizations of the height profile for different film thicknesses.

2 Dynamics of the growth process

The solution of the nonlinear evolution equation exhibits some unexpected initial linear behavior. This can be explained by an appropriate decomposition of the spectrum $\sigma \subset \mathbb{R}$ of the associated linearized operator which is self-adjoint and sectorial. In particular, we specify three constants

$$\gamma^{--} < 0 < \gamma^{+} < \gamma^{++} < 1$$

such that, referring to λ_{max} as the maximum eigenvalue, the spectrum is decomposed into the four parts

$$\begin{aligned} \sigma^{--} &:= (-\infty, \gamma^{-}\lambda_{max}) \quad , \quad \sigma^{-} := (\gamma^{-}\lambda_{max}, \gamma^{+}\lambda_{max}) \quad , \\ \sigma^{+} &:= (\gamma^{+}\lambda_{max}, \gamma^{++}\lambda_{max}) \quad , \quad \sigma^{++} := (\gamma^{++}\lambda_{max}, +\infty) \quad . \end{aligned}$$

We further denote by X^{--} , X^{-} , X^{+} and X^{++} the subspaces spanned by the corresponding eigenfunctions:

$$\begin{aligned} X^{--} &:= \text{span}\,\{\varphi(\lambda) \mid \lambda \in \sigma^{--}\} \quad , \quad X^{-} := \text{span}\,\{\varphi(\lambda) \mid \lambda \in \sigma^{-}\} \, , \\ X^{+} &:= \text{span}\,\{\varphi(\lambda) \mid \lambda \in \sigma^{+}\} \quad , \quad X^{++} := \text{span}\,\{\varphi(\lambda) \mid \lambda \in \sigma^{++}\} \, . \end{aligned}$$

Then, the direct sum of X^{+} and X^{++} can be shown to be a dominant subspace which determines the dynamical behavior of solutions to the nonlinear evolution equation in the following sense:

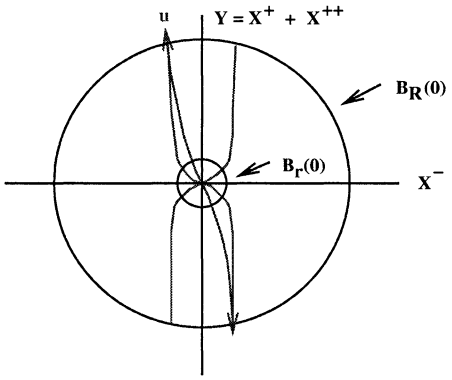

Fig. 2. Illustration of the initial linear behavior of the solution

Theorem 1. *Assume* $u(\cdot,0) \in H^3(\Omega)$ *with*

$$\|u(\cdot,0)\|_{2,\Omega} \leq r := C\, L^{3-\alpha}\ ,\ \alpha > 0\quad ,$$

and set

$$\bar{u}^0 := L^{-2} \int_{\Omega} u_0(x)\, dx\quad .$$

Then there exists $t^* > 0$ *such that the solution* $u = u(x,t), x \in \Omega, t \in [0,t^*)$, *of* (6) *stays with probability 1 in a vicinity of the dominant subspace*

$$Y := \bar{u}^0 + X^+ \oplus X^{++} \tag{7}$$

until at $t = t^*$ *it leaves a ball* $B_R(0)$ *with radius* $R > r$.

Proof. For a proof of this result we refer to [2].

Figure 2 illustrates the initial linear behavior of the solution in case $\bar{u}_0 = 0$. We note that a related result for the Cahn-Hilliard equation has been established in [12].

3 Spectral Galerkin approximation

For the spectral Galerkin approximation we consider the weak formulation of the implicitly in time discretized nonlinear evolution equation which involves the Sobolev space $V := H^2_{per}(\Omega)$ in case of periodic boundary conditions and $V := H^2(\Omega)$, if homogeneous Neumann boundary conditions are imposed. Using the backward Euler scheme and denoting by $u^m \in V$ an approximation of $u(\cdot,t_m)$ at time t_m and by $\tau_m := t_m - t_{m-1}$ the time step from level $m-1$ to level m, the problem is as follows: Find $u^m \in V$ such that for all $\chi \in V$

$$\int_\Omega u^m \chi dx = \int_\Omega u^{m-1} \chi dx + \tau_m \int_\Omega [a_1 u^m + a_2 \Delta u^m + f(u^m)] \Delta \chi dx \ , \qquad (8)$$

where the nonlinearity $f(u^m)$ is given by $f(u^m) := a_3 |\nabla u^m|^2$.
We refer to λ_i , $1 \leq i \leq N$, as the first N eigenvalues of $-\Delta$ and denote by $V_N := \text{span } \{\varphi_i \mid 1 \leq i \leq n\}$ the finite dimensional subspace of V spanned by the associated orthonormal eigenfunctions.
The spectral Galerkin approximation is then a linear combination $u_N^m = \sum_{k=1}^{N} u_{N,i}^m \varphi_i \in V_N$ so that (8) with V replaced by V_N gives rise to the nonlinear system

$$g_i(u_N^m) = (1 + a_1 \tau_m \lambda_i - a_2 \tau_m \lambda_i^2) u_{N,i}^m + \qquad (9)$$
$$+ \tau_m \lambda_i \int_\Omega f(\sum_{k=1}^{N} u_{N,k}^m \varphi_k) \varphi_i \, dx - u_{N,i}^{m-1} = 0 \quad , \quad 1 \leq i \leq N \quad .$$

The solution of that nonlinear system by Newton's method would be quite expensive, since it requires the computation of the Jacobian at each iteration step. It turns out that it is sufficient to use the method of successive iterations which corresponds to the approximation of the original problem by the semi-implicit Euler Scheme: For $\nu \geq 0$ compute $u_N^{m,\nu} \in V_N$ as the solution of

$$\int_\Omega u_N^{m,\nu} \chi_N \, dx = \int_\Omega u_N^{m-1} \chi_N \, dx + \tau_m \int_\Omega [a_1 u_N^{m,\nu} + \qquad (10)$$
$$+ a_2 \Delta u_N^{m,\nu} + f(u_N^{m,\nu-1})] \Delta \chi_N \, dx \quad , \quad \chi_N \in V_N \quad ,$$

where $u_N^{m,-1} := u_N^{m-1}$. In this case, we can explicitly solve for the components of the new iterate

$$u_{N,i}^{m,\nu} = \frac{u_{N,i}^{m-1} - \tau_m \lambda_i f_i^{m,\nu-1}}{1 + a_1 \tau_m \lambda_i - a_2 \tau_m \lambda_i^2} \quad , \quad 1 \leq i \leq N \quad , \qquad (11)$$

where

$$f_i^{m,\nu-1} := \int_\Omega f(\sum_{k=1}^{N} u_{N,k}^{m,\nu-1} \varphi_k) \, \varphi_i \, dx \quad , \quad 1 \leq i \leq N \quad .$$

We only have to evaluate the nonlinear terms $f_i^{m,\nu-1}$ which can be efficiently done by the Fast Fourier Transform in case of periodic boundary conditions and by the Fast Cosine Transform for homogeneous Neumann boundary conditions. In both cases, this is done with respect to an equidistant grid consisting of M^2 grid points where M has to be chosen larger than the dimension of the trial space V_N in order to avoid aliasing effects.

The semi-implicit Euler scheme is carried out with an automatic step-size control. The error due to the time discretization is estimated by

$$\gamma \, \|\tilde{u}^m - u^m\| \leq \|u(t_m) - u^m\| \leq \Gamma \, \|\tilde{u}^m - u^m\| \quad ,$$

where $\tilde{u}^m \in V$ is the solution of the semi-implicit trapezoidal rule

$$\int_\Omega \tilde{u}^m \chi dx = \int_\Omega u^{m-1} \chi dx + \frac{\tau_m}{2} \int_\Omega \left[a_1 (\tilde{u}^m + u^{m-1}) + \right. \tag{12}$$
$$\left. + a_2 \Delta (\tilde{u}^m + u^{m-1}) + (f(u^m) + f(u^{m-1})) \right] \Delta \chi dx \ , \ \chi \in V \ .$$

If $V = V_N$, the solution of (12) can be easily computed according to

$$(\tilde{u}_N^m)_i = (u_N^{m-1})_i - \frac{\tau_m}{2} \left[a_1 \, \lambda_i \, ((\tilde{u}_N^m)_i + (u_N^{m-1})_i) - \right.$$
$$\left. - \, a_2 \, \lambda_i^2 \, ((\tilde{u}_N^m)_i + (u_N^{m-1})_i) - \lambda_i \, (f_i^m + f_i^{m-1}) \right] \ , \ 1 \leq i \leq N \ .$$

In the practical realization of the step-size control, we additionally take into account the error due to the discretization in space. The error $\|u^m - u_N^m\|_{2,\Omega}$ is caused by the negligence of those eigenmodes $i > N$ that have not been considered in the spectral Galerkin approximation, but are relevant for the exact computation of the nonlinearities. Therefore, for sufficiently large P, we set

$$e_{u_N^m} = \sum_{N<j<N+P} \frac{\tau_m \, \lambda_j \, f_j^m}{1 + a_1 \, \tau_m \, \lambda_j - a_2 \, \tau_m \, \lambda_j^2}$$

Given a tolerance $tol > 0$, we check for convergence:

$$\frac{\|\tilde{u}_N^m - u_N^m\|_{2,\Omega} + (\sigma^{-1} - 1) \, |e_{u_N^m}|}{\|\tilde{u}_N^m\|_{2,\Omega}} \leq tol \quad , \tag{13}$$

where $\sigma < 1$ is an appropriate weighting factor. If (13) is satisfied we proceed with the new time-step

$$\bar{\tau}_m := \sqrt{\frac{\sigma \, tol \, \|\tilde{u}_N^m\|_{2,\Omega} - |e_{u_N^m}|}{\|\tilde{u}_N^m - u_N^m\|_{2,\Omega}}} \quad . \tag{14}$$

Otherwise, we repeat the previous time-step with $\bar{\tau}_m$.

4 The finite element method

The spectral Galerkin method becomes inefficient when the nonlinear dynamics sets in, i.e., when the solution leaves the dominant subspace Y as given by (7). Although a theoretical bound for the exit time t^* is known (cf., e.g., [2]),

this bound is an overestimation and hence not practicable. Therefore, we stop the spectral approach and switch to a finite element method, if the convergence test (13) fails for several consecutive time-steps.
The finite element approximation is based on a reformulation of the 4th order equation (6) as a system of two 2nd order equations

$$\left.\begin{aligned} \partial u/\partial t &= \Delta w \\ w &= a_1 u + a_2 \Delta u + a_3 |\nabla u|^2 \end{aligned}\right\} \quad \text{in } Q := \Omega \times [0,\infty) \tag{15}$$

We discretize in time by the implicit Euler method and in space by continuous, piecewise linear finite elements with respect to a simplicial triangulation $\mathcal{T}_h$ of Ω. Denoting by $S_1(\Omega;\mathcal{T}_h)$ the associated finite element space, for each time-step we have to solve the nonlinear system of equations:
Find $(u_h^m, w_h^m) \in S_1(\Omega;\mathcal{T}_h) \times S_1(\Omega;\mathcal{T}_h)$ such that

$$\int_\Omega \frac{u_h^m - u_h^{m-1}}{\tau_m} \chi_h \, dx + \int_\Omega \nabla w_h^m \cdot \nabla \chi_h \, dx = 0 \,, \quad \chi_h \in S_1(\Omega;\mathcal{T}_h) \,, \tag{16}$$

$$a_1 \int_\Omega u_h^m \psi_h \, dx - a_2 \int_\Omega \nabla u_h^m \cdot \nabla \psi_h \, dx + a_3 \int_\Omega |\nabla u_h^m|^2 \psi_h \, dx - \tag{17}$$

$$- \int_\Omega w_h^m \psi_h \, dx = 0 \,, \quad \psi_h \in S_1(\Omega;\mathcal{T}_h) \,.$$

Providing a hierarchy $(\mathcal{T}_{h_i})_{i=0}^{\ell}$ of triangulations, we solve the nonlinear system (16), (17) on the finest grid by Newton-Multigrid:
Given $(u_\ell^{m,\nu}, w_\ell^{m,\nu}) \in S_1(\Omega;\mathcal{T}_\ell) \times S_1(\Omega;\mathcal{T}_\ell)$, we compute

$$u_\ell^{m,\nu+1} = u_\ell^{m,\nu} + \delta_{u_\ell}^{m,\nu} \quad , \quad w_\ell^{m,\nu+1} = w_\ell^{m,\nu} + \delta_{w_\ell}^{m,\nu} \quad ,$$

where the Newton increment $(\delta_{u_\ell}^{m,\nu}, \delta_{w_\ell}^{m,\nu})$ is the solution of the linear system

$$\int_\Omega \delta_{u_\ell}^{m,\nu} \chi_\ell dx + \tau_m \int_\Omega \nabla \delta_{w_\ell}^{m,\nu} \cdot \nabla \chi_\ell dx = \int_\Omega u_\ell^{m-1} \chi_\ell dx - \tag{18}$$

$$- \int_\Omega u_\ell^{m,\nu} \chi_\ell dx - \tau_m \int_\Omega \nabla w_\ell^{m,\nu} \cdot \nabla \chi_\ell dx \quad , \quad \chi_\ell \in S_1(\Omega;\mathcal{T}_{h_\ell} \,,$$

$$\int_\Omega \delta_{w_\ell}^{m,\nu} \psi_\ell dx - a_1 \int_\Omega \delta_{u_\ell}^{m,\nu} \psi_\ell dx + a_2 \int_\Omega \nabla \delta_{u_\ell}^{m,\nu} \cdot \nabla \psi_\ell dx - \tag{19}$$

$$- \int_\Omega f'(u_\ell^{m,\nu}) \delta_{u_\ell}^{m,\nu} \psi_\ell dx = - \int_\Omega w_\ell^{m,\nu} \psi_\ell dx + a_1 \int_\Omega u_\ell^{m,\nu} \psi_\ell dx -$$

$$- a_2 \int_\Omega \nabla u_\ell^{m,\nu} \cdot \nabla \psi_\ell dx + \int_\Omega f(u_\ell^{m,\nu}) \psi_\ell dx \quad , \quad \psi_\ell \in S_1(\Omega;\mathcal{T}_{h_\ell} \,.$$

The system (18),(19) is solved by linear multigrid using incomplete LU decomposition both as smoother on all levels $1 \leq i \leq \ell$ as well as an iterative solver for the coarse grid correction equation on level $i = 0$.
For the finite element approach we use a similar step-size control as in case of the spectral Galerkin method, except that we replace the estimation of the error due to the discretization in space by a residual-type a posteriori error estimator.

5 Simulation results

We have used the combined spectral element/finite element approach for the numerical simulation of the deposition of the metallic glassy film $ZrAlCu$ on silicon substrates.
The computational domain Ω has been chosen as a square of length $L = 200nm$ in each direction. Periodic boundary conditions have been imposed and the initial height profile $u_0(x)$, $x \in \Omega$ has been determined randomly with $\bar{u}_0 = 0$.
In the spectral element approach we have used 125, 200, and 250 modes per dimension, whereas for the computation of the nonlinearities by the Fast Fourier Transform a uniform grid with $M = 400$ grid points in each direction has been employed which is sufficiently large to avoid aliasing effects.
In the finite element method we used a hierarchy $(\mathcal{T}_\ell)_{k=0}^4$ of five simplicial triangulations with $h_0 = 1/25$ and $h_4 = 1/400$.

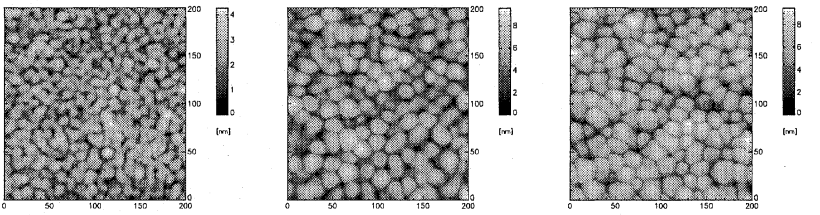

Fig. 3. Computed height profile for different film thicknisses [100 nm (left), 360 nm (middle), and 480 nm (right)]

Figure 3 displays the computed height profiles for different film thicknesses in a grey scale ranging from black (0 nm) to white (4 nm). One clearly observes the effect of structure coarsening: a surface pattern with a mesa-like structure evolves featuring hills with flat plateaus that are separated by narrow deep valleys. We note that already for 125 modes per dimension the computed profiles are both qualitatively and quantitatively in good agreement with experimentally obtained data (cf., e.g., [11]).

Acknowledgement. The work of the authors has been supported by the German National Science Foundation (DFG) within the Collaborative Research Center SFB 438 and the Graduate School GK 283.

References

1. A.L. Barabasi, and H.E. Stanley (1995): Fractal Concepts in SurfaceGrowth. Cambridge Univ. Press Cambridge
2. D. Blömker (2000): Stochastic Partial Differential Equations and Surface Growth. Wissner Augsburg
3. R.H.W. Hoppe, W.G. Litvinov, S.J. Linz (2003): On solutions of certain classes of evolution equations for surface morphologies. Journal of Nonlinear Phenomena in Complex Systems **6**, 582–591
4. M. Kardar, G. Parisi, Y.-C. Zhang (1986): Dynamic scaling of growing interfaces. Phys. Rev. Lett. **56**, 889–892
5. S.J. Linz, M. Raible, and P. Hänggi (2000): Stochastic field equation for amorphous surface growth. Lecture Notes in Physics **557**, 473–483
6. S. Maier-Paape, T. Wanner (2000): Spinodal decomposition for the Cahn-Hilliard equation in higher dimensions: Nonlinear dynamics. Arch. Rat. Mech. Anal. **151**, 187–219
7. E.M. Nash (2001): Finite-Elemente und Spektral-Galerkin Verfahren zur numerischen Lösung der Cahn-Hilliard Gleichung und verwandter nichtlinearer Evolutionsgleichungen. Shaker Aachen
8. Ch.-D. Nguyen (2003): Level set methods for nonlinear deposition equations. Dissertation. Institute for Mathematics, University of Augsburg
9. Ch.-D. Nguyen, R.H.W. Hoppe (2003): Amorphous surface growth via a level set approach. submitted to Nonlinear Analysis: Theory, Methods, and Applications
10. M. Raible, S.J. Linz, P. Hänggi (2000): Amorphous thin film growth: Minimal deposition equation. Phys. Rev. E **62**, 1691–1705
11. M. Raible, S.G. Mayr, S.J. Linz, M. Moske, P. Hänggi, K. Samwer (2000): Amorphous thin film growth: theory compared with experiment. Europhys. Lett. **50**, 61–67
12. E. Sander, T. Wanner (2000): Unexpectedly linear behavior for the Cahn-Hilliard equation. SIAM J. Appl. Math. **60**, 2182–2202
13. D.E. Wolf, J. Villain (1990): Growth with surface diffusion. Europhys. Lett. **13**, 389–394